Linear Overmodulation Strategy for Current Control in Photovoltaic Inverter

Yongsoon Park, *Member, IEEE*, Seung-Ki Sul, *Fellow, IEEE*, and Ki-Nam Hong

***Abstract*—The maximum power point should be continuously tracked in a photovoltaic (PV) inverter. However, the maximum power point could be found at very low dc-link voltages around sunrise or sunset. Then, the overmodulation (OVM) of the inverter has to be considered to keep the power generation even at low dc-link voltages. In this paper, a series of implementation schemes is proposed to keep the current regulation, even if the inverter is under the OVM. These schemes can be helpful to increase the operating time of the PV inverter, which correlates with the daily amount of power generation. After being examined in a small-scale prototype inverter, the proposed method has been tested with a 250-kW PV inverter installed at a proving ground. In a sunset, the operation time of the inverter has been extended by about 12 min, and the generated energy has been increased by 234 Wh, when compared to the normal operation without the proposed methods.**

***Index Terms*—Current control, overmodulation (OVM), photovoltaic (PV) inverter.**

I. Introduction

LARGE-SCALE photovoltaic (PV) inverters are commonly connected to a three-phase utility grid. In this type of grid-connected inverter, the dc-link voltage has to be larger than a certain limit for the stable operation. The PV panel connected to the dc link can be constructed, such that the maximum power point tracking (MPPT) is mostly achieved in a voltage range well above the voltage limit. However, depending on irradiance and temperature, the actual maximum power point may be placed below the voltage limit.

Usually, the lowest dc-link voltage limit is determined by a manufacturer with considering some design margin for the stable operation of PV inverters. If the dc-link voltage becomes lower than this minimum voltage limit, the PV inverter stops operation itself. Above all, the reconnection to the grid after stop of operation is quite time consuming. In particular, if the maximum power point to be tracked fluctuates near the lower limit, then the inverter's outage would be frequent. It could be a loss to disconnect the inverter from the grid whenever the dc-link voltage crosses the lower limit. This is because the limiting value is conservatively set with an enough margin. Definitely, if possible, this type of outage should be prevented for the consistent operation of the PV inverter.

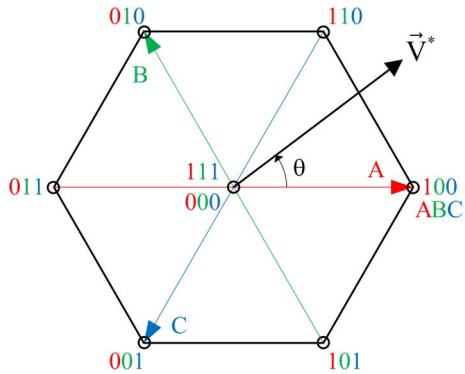

Fig. 1. Voltage reference vector and voltage hexagon.

The primary reason to disconnect the inverter at low dc-link voltages is that the voltage output cannot be correctly synthesized in accordance with its reference. As shown in Fig. 1, a voltage hexagon can be drawn for a three-phase inverter [1]. This hexagon indicates the area where a three-phase voltage reference can be properly synthesized. However, because the hexagon size is proportional to the dc-link voltage, the reference to be synthesized can be placed outside the hexagon if the dc-link voltage is excessively reduced. Therefore, the overmodulation (OVM) becomes important at low dc-link voltages in PV inverters.

One category of OVM is to modify the spatial position of the reference vector in the voltage plane partitioned by the hexagon [1]–[6]. In the other category, OVM is applied by simply saturating the pole voltages to the half of the dc-link voltage [7]–[9]. On the other hand, in this paper, OVM is discussed from the perspective of modification of the switching function. On the basis of this insight, several candidates for OVM are considered. In particular, the output current of the grid-connected inverter has to be regulated in terms of harmonics [10]. However, the occurrence of harmonic currents is inevitable in OVM. Therefore, depending on operating conditions, the suitable selection of OVM method is discussed to minimize the harmonic currents into the grid.

In addition to the harmonics, the fundamental currents should be properly regulated by feedback loops for the modulation of active and reactive powers. This feedback control also should

Manuscript received August 14, 2014; revised December 30, 2014 and June 5, 2015; accepted July 23, 2015. Date of publication August 25, 2015; date of current version January 18, 2016. Paper 2014-IPCC-0575.R2, presented at the 2014 International Power Electronics Conference (IPEC-Hiroshima 2014 ECCE-Asia), Hiroshima, Japan, May 18–21, and approved for publication in the IEEE TRANSACTIONS ON INDUSTRY APPLICATIONS by the Industrial Power Converter Committee of the IEEE Industry Applications Society.

Y. Park was with the Department of Electrical and Computer Engineering, Seoul National University, Seoul 151-744, Korea. He is now with Samsung Electronics Company, Ltd., Suwon 442-600, Korea (e-mail: sulsk@plaza.snu.ac.kr).

S.-K. Sul is with the Department of Electrical and Computer Engineering, Seoul National University, Seoul 151-744, Korea (e-mail: sulsk@plaza.snu.ac.kr).

K.-N. Hong is with LG Electronics, Inc., Incheon 404-170, Korea (e-mail: hong0093@hanmail.net).

Color versions of one or more of the figures in this paper are available online at http://ieeexplore.ieee.org.

Digital Object Identifier 10.1109/TIA.2015.2472518

be effective, even if the inverter is under OVM. Moreover, since the fundamental output of the inverter is limited under a finite dc-link voltage, it is essential to consider the antiwindup of integrators used in the feedback control loop of the current regulator [11]. By considering these points, a design method for PV inverters with current regulation loop is proposed in this paper. By virtue of the proposed method, the power factor of the fundamental currents can be aptly maintained, even if the voltage output is limited in OVM.

The performance of the proposed methods is fundamentally confirmed with a laboratory-scale prototype inverter. Then, the feasibility and performance of the proposed method are discussed with the results obtained from a 250-kW PV inverter installed in the Gochang proving ground, South Korea.

II. OVM Method

The voltage reference has to be modified when the inverter is under OVM. In order to minimize the error caused by this modification, the modified reference by OVM should be located on a side of the hexagon.

In general, a reference vector is synthesized by (1), according to space vector pulsewidth modulation (SVPWM) [12]. That is,

$$\vec{V}^* = \frac{1}{T_s}(\vec{V}_1 \cdot T_1 + \vec{V}_2 \cdot T_2 + \vec{V}_0 \cdot T_0). \tag{1}$$

However, the zero vector denoted by $\vec{V}_0$ in (1) is useful for PWM only if the reference vector is inside the hexagon. In other words, if the modified reference by OVM is on a side of the hexagon, T_0 in (1) becomes null, and only the effective vectors at the hexagon vertices in Fig. 1 are used for PWM. In the figure, the switching functions, which indicate the ON-state of the upper switch in a leg, are also presented for each vector. The switches in the same leg operate complementary. In the switching function, "1" stands for the ON-state of the upper switch while "0" for the OFF-state.

By considering the switching functions, the variation of the pole voltages can be partially inferred when the reference vector rotates along the hexagon. For example, if the reference vector is on the hexagon side from 0 to $\pi/3$ in Fig. 1, both of the effective vectors have the same switching function for A-phase, which corresponds to unity. Because the zero vector is not used at all for the reference on the hexagon side, the upper switch of A-phase is always turned on for the phase range of concern. By extending this knowledge, the pole voltage reference for A-phase can be drawn, as shown in Fig. 2, when the reference vector rotates once along the hexagon. The ranges where the switching function can be changed are indicated by the dashed boxes.

From Fig. 2, it can be inferred that the pole voltages are fixed for some phase ranges, regardless of OVM methods, if the modified reference is on the hexagon sides. In other words, OVM methods can be differentiated by how the connections between "a" and "b" points and between "c" and "d" points are made. Then, three OVM methods could be simply introduced, as shown in Fig. 3. Their common properties are piecewise straight lines and odd function with respect to the center point

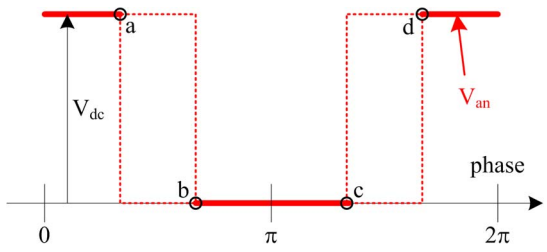

Fig. 2. A-phase pole voltage (V_{an}) under OVM for a fundamental period.

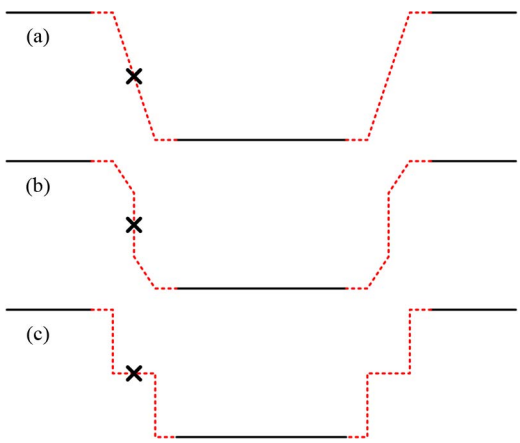

Fig. 3. A-phase pole voltage (V_{an}) under various OVM methods: (a) OVM1, (b) OVM2, and (c) OVM3.

"x," which can respectively contribute to simple implementation and prevention of even harmonics. Almost the same patterns with OVM1 and OVM2 can be observed, when the pole voltages are saturated at the half of the dc-link voltage, under SVPWM and Depenbrock's discontinuous PWM, respectively [7]. The three methods in Fig. 3 have been initially considered for OVM in this paper, due to their simple implementation. However, other diverse OVM methods can be further derived on the basis of Fig. 2.

For the grid connection of an inverter, OVM methods should be evaluated, in terms of their harmonic property, to meet the harmonic standards [10]. The weighted total harmonic distortion (WTHD) of the voltage can be a useful tool to compare the degree of harmonic current into the grid without any information on filter inductance [13]. In each OVM method, the WTHD has been computed, with respect to the voltage reference, instead of pulsewidth-modulated waveforms. This was intended to insightfully discuss the harmonic distortions, regardless of the sampling frequency. The WTHDs of the three OVMs in Fig. 3 are shown in Fig. 4, according to the modulation index (MI), along with that of another method denoted by OVM4, which will be described in Section II-A. As shown in Fig. 4, the WTHD of each OVM method varies over the entire OVM range, where the MI is from $2/\sqrt{3}$ to $4/\pi$. In this paper, MI is defined as the ratio of the fundamental voltage to the half of the dc-link voltage.

In fact, the WTHDs in Fig. 4 are almost the same with the weighted selective harmonic distortions (WSHDs) shown in Fig. 5, which only consider 5th-, 7th-, 11th-, and 13th-order

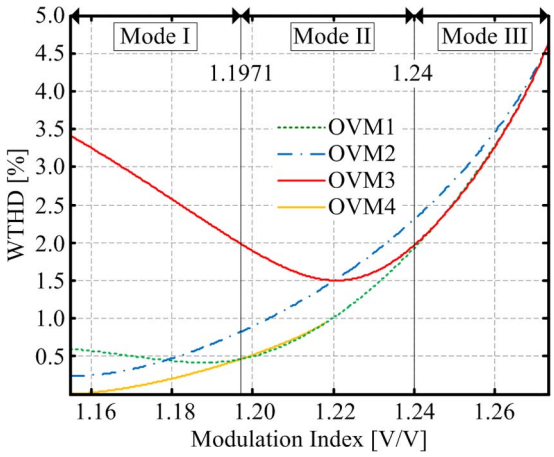

Fig. 4. WTHDs for OVM methods.

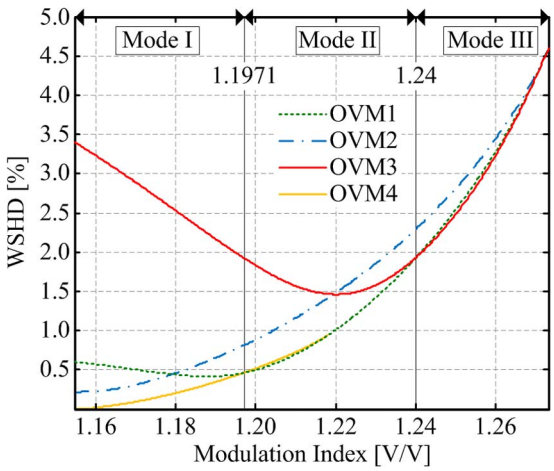

Fig. 5. WSHDs for OVM methods.

harmonics. That is, the main harmonic orders affected by OVM are thought to be smaller than 15. The further consideration of the other higher harmonics to an LCL filter resonance might be beyond the scope of this paper. In addition, although WTHD considers an infinite order of harmonics, the maximum harmonic order of concern must be limited because the sampling frequency for PWM was disregarded, as mentioned earlier. Therefore, the following discussions are advanced with WSHDs of the main low-order harmonics. If the system design should be more customized with a specific sampling frequency, it would be accurate to use the WTHD of pulsewidth-modulated waveforms for analysis, at the expense of large computation effort.

OVM can be differently implemented, depending on MI, under the considerations of Fig. 5, to minimize the harmonic distortions. Then, OVM modes can be divided into three by the intersections of the WSHD lines in Fig. 5. Namely, OVM4 is selected in Mode I range, OVM1 in Mode II range, and OVM3 in Mode III range.

When it comes to the employment of OVM4, it should be noted that all OVM methods in Fig. 3 force the modified reference to be on the hexagon sides. However, as shown in

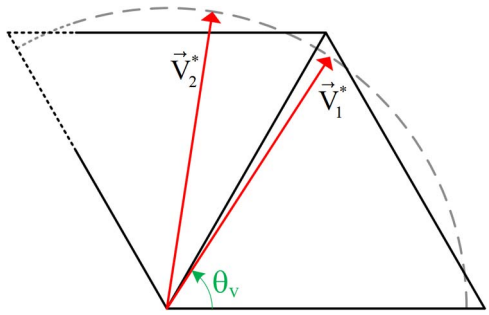

Fig. 6. Voltage reference vector when MI is between $2/\sqrt{3}$ and 4/3.

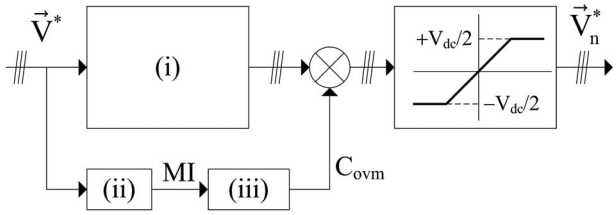

Fig. 7. Implementation of OVM1 and OVM4 methods.

Fig. 6, the original reference before OVM can be inside or outside the hexagon during the rotation, when its MI is between $2/\sqrt{3}$ and 4/3. In particular, if the original reference is almost inside the hexagon during the rotation, the application of OVM methods in Fig. 3 would be excessive. This is because they uniformly force the modified reference to be on the hexagon sides, even if the original one is inside the hexagon. Thus, the other method denoted by OVM4 in Fig. 5, which is detailed in the following section, can be considered to minimize the harmonic distortions, when MI is close to $2/\sqrt{3}$, under OVM.

It is described in detail, in the following sections, how to implement OVM in each mode. In addition, it should be noted that OVM1, OVM2, and OVM3 are the simple examples of OVM methods based on Fig. 2. The possibility to further minimize WSHD under OVM is still open, if another method is considered under the insight of Fig. 2. Thus, if the better method is found, its application range can be determined according to the same criterion.

A. *OVM Mode I*

The magnitude error under OVM is minimized by moving an original reference toward the direction normal to the hexagon side [3]. This OVM method can be simply implemented by limiting the voltage references after SVPWM [14], [15], and this can be explained with Fig. 7 when the multiplication of $C_{\rm ovm}$ is ignored. Namely, SVPWM is applied to the original reference $\vec{V}^*$ by stage (i), and the limiter works if the reference modified by SVPWM is greater than $V_{\rm dc}/2$ or smaller than $-V_{\rm dc}/2$. However, when this limiting occurs, the final reference $\vec{V}_n^*$ becomes smaller than the original reference at the fundamental frequency. This magnitude reduction at the fundamental frequency can deteriorate the dynamic performance of the current regulation.

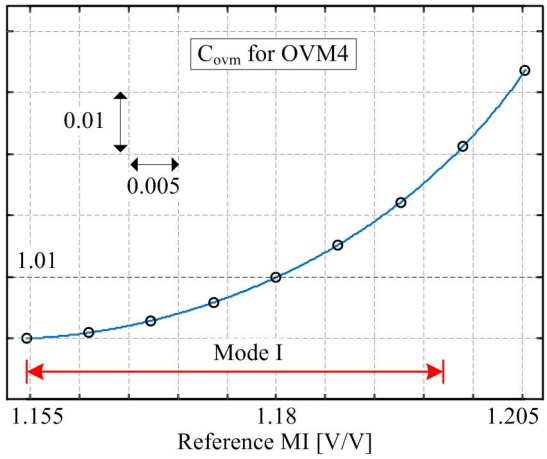

Fig. 8. $C_{\rm ovm}$ table for OVM4.

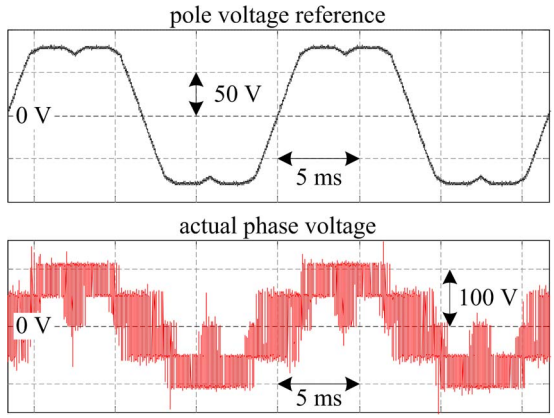

Fig. 9. Pole and phase voltages when MI is 1.1812.

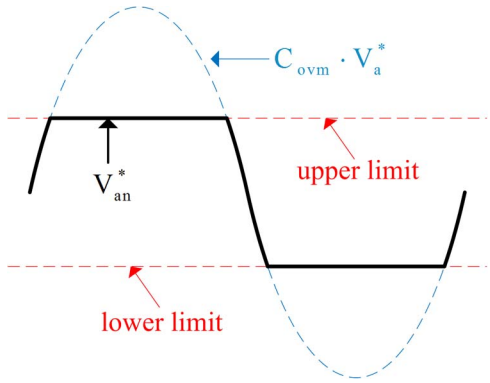

Fig. 10. Pole voltage generation in OVM mode II.

Then, stages (ii) and (iii) are necessary to make the original and final references to be the same at the fundamental frequency. In stage (ii), the MI of the original reference is detected from $\vec{V}^*$ and the dc-link voltage. Then, in stage (iii), the appropriate gain denoted by $C_{\rm ovm}$ is found from Fig. 8, according to the detected MI. That is, if the voltage reference after stage (i) is compensated by $C_{\rm ovm}$, the final reference saturated by the limiter can present the same fundamental magnitude with the original reference before stage (i). This OVM method including the gain compensation is denoted by OVM4 in Figs. 4 and 5. Meanwhile, through stage (ii), which OVM mode has to be applied can be also determined by the detected MI.

The values for $C_{\rm ovm}$ in Fig. 8 have been numerically obtained by computer simulations. Namely, in Fig. 7, the original reference processed by SVPWM was directly saturated by the limiter when stages (ii) and (iii) were disregarded. Then, the actual MI of the final reference could be collected in terms of the fundamental frequency. For instance, when the original reference MI was 1.1918, the actual MI was measured as 1.18. In reverse, this means that an actual MI of 1.18 can be achieved with a fictitious MI of 1.1918. Therefore, the necessary gain for compensation $C_{\rm ovm}$ is computed as $1.01\ (=1.1918/1.18)$. Through this principle, all the gains in Fig. 8 have been computed. In practical implementation, only the points indicated by circles in Fig. 8 are stored in the table, while the other values are linearly interpolated.

As an example, the pole voltage reference and the actual phase voltage under OVM4 have been captured, as shown in Fig. 9, when the reference MI was 1.1812 and $V_{\rm dc}$ was 160 V. In the frequency analysis on Fig. 9, the actual fundamental voltage was 93.61 V, which reveals only -0.94% error to the original reference (see $\vec{V}^*$ in Fig. 7).

B. OVM Mode II

According to Fig. 5, when the reference MI is between 1.1971 and 1.24, OVM1 is applied to modify the voltage reference outside the hexagon. The process of OVM1 can be also understood with Fig. 7. In fact, when it comes to the pole voltage, OVM4 becomes almost equal to OVM1 when MI approaches to $4/\pi$ [7]. However, by utilizing a different gain table, stage (i), where SVPWM had to be carried out in OVM4, can be skipped in OVM1. This means that the implementation effort can be reduced by using OVM1 when compared to OVM4. For the implementation of OVM1, a quasi-trapezoidal voltage can be generated by limiting an amplified sinewave, as shown in Fig. 10. This simple scheme has been adopted because sinewaves present almost linear variations near zero crossings. Then, with the bypass of stage (i) in Fig. 7, OVM1 can be implemented with Fig. 11, which was obtained through the same way as that in Fig. 8.

In order to show an example in OVM mode II, the pole voltage reference and the actual phase voltage have been captured, as shown in Fig. 12, when the reference MI is 1.225, under the same $V_{\rm dc}$, i.e., 160 V. In the frequency analysis, the actual fundamental voltage was 97.44 V, which means -0.57% error to the original reference.

C. OVM Mode III

Both OVM1 and OVM4 have a demerit when the six-step operation is required. Theoretically, this is because their compensation gains must be infinity to implement the six-step operation. Furthermore, because harmonic currents can be reflected into the voltage references by the current regulation under OVM, the infinite gain can amplify these harmonics as

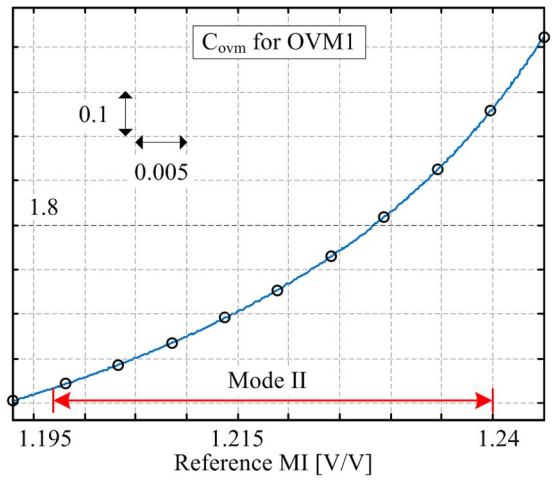

Fig. 11. $C_{\rm ovm}$ table for OVM1.

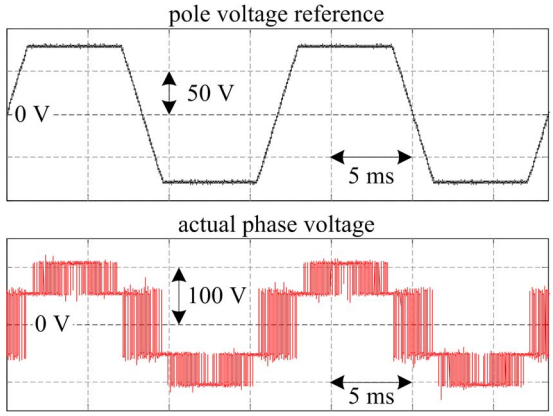

Fig. 12. Pole and phase voltages when MI is 1.225.

Fig. 13. A-phase pole voltage under OVM3.

well. In addition, OVM3 presents slightly better WSHDs in Fig. 5, when MI is greater than 1.24.

The phase angle denoted by α in Fig. 13 is the main factor to adjust the fundamental voltage in OVM3. When α decreases, the MI for the fundamental voltage and the WSHD increase simultaneously. In particular, if α becomes zero, the inverter is under the six-step operation. The required α according to MI has been numerically obtained, as shown in Fig. 14.

The voltage synthesis under OVM3 has been captured as shown in Fig. 15 when MI is 1.263 under the same $V_{\rm dc}$, 160 V. In the frequency analysis, the actual fundamental voltage was 100.7 V, which means -0.297 % error to the original reference. The phase voltage in Fig. 15 is very close to the six-step operation.

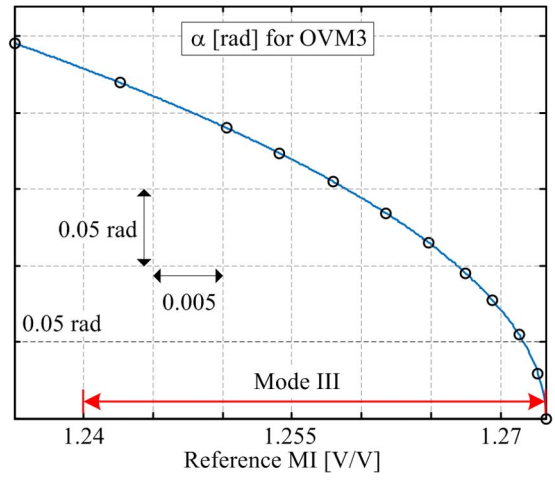

Fig. 14. α table for OVM3.

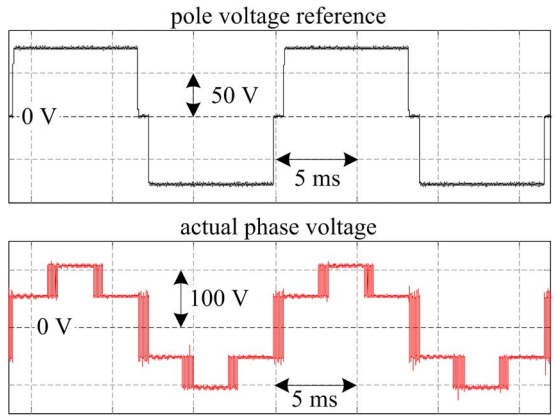

Fig. 15. Pole and phase voltages when MI is 1.625.

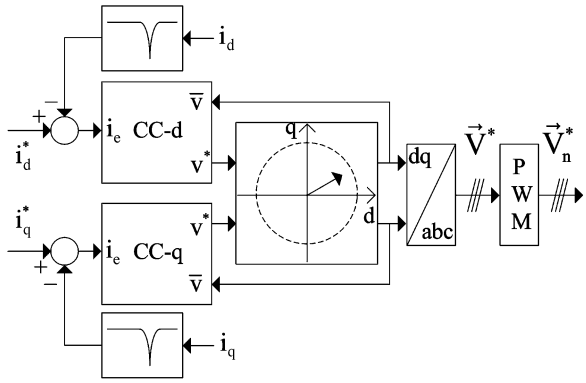

Fig. 16. Current control structure.

III. Current Control Under OVM

In grid-connected PV inverters, the feedback control on output currents at the fundamental frequency should be kept, even under OVM, to regulate active and reactive powers, which are transferred to the grid [16]. The proposed current control can be understood with Figs. 16 and 17.

As mentioned earlier, low-order harmonic currents can be reflected into voltage references through the feedback control under OVM. If these harmonics are not aptly mitigated, the

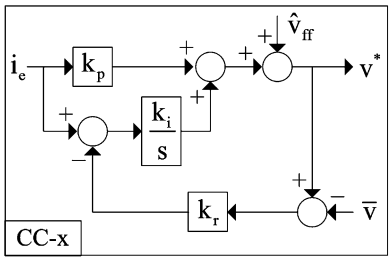

Fig. 17. Current controller.

actual voltage outputs of the inverter would be more distorted. To deal with this problem, notch filters explained with (2) could be used to mitigate harmonic distortions in the synchronous reference frame. Through these notch filters, voltage references can be less distorted under OVM. Hence,

$$\mathrm{NF}(s) = \frac{s^2 + \omega_{\mathrm{nf}}^2}{s^2 + 2\zeta\omega_{\mathrm{nf}} s + \omega_{\mathrm{nf}}^2}. \tag{2}$$

The notch frequency ω_{nf} in (2) can be set to $2\pi 360$ rad/s, to deal with the 5th- and 7th-order harmonics in the synchronous reference frame. In order to set the damping coefficient ζ in (2), the current control property has been considered together. The current controller in the synchronous reference frame can be designed to present the following closed-loop response [17]:

$$\mathrm{CC}(s) = \frac{\omega_{\mathrm{cc}}}{s + \omega_{\mathrm{cc}}} \tag{3}$$

where ω_{cc} is the control bandwidth.

This response is possible only if the pole-zero cancelation is correct with the following proportional–integral (PI) gains:

$$k_p = L\omega_{\mathrm{cc}}, \quad k_i = R\omega_{\mathrm{cc}} \tag{4}$$

where L and R are line inductance and resistance between a PV inverter and the grid.

If harmonic controllers such as resonant controller are separately used [18], the control bandwidth for the fundamental current should be limited, to prevent interferences between the fundamental and harmonic current controllers. Then, ω_{cc} in (3) can be empirically set below $2\pi 200$ rad/s, to prevent the interference. Because the notch filters are employed on the feedback loops, as presented in Fig. 16, their response should not disturb the original loop property. As shown in Fig. 18, if ζ is set as 0.1 rather than 1, the magnitude and phase of notch filter can be almost 0 dB and 0°, respectively, within the bandwidth of current control. Because 0 dB and 0° in the Bode plot means no disturbance in magnitude and phase, ζ was set as 0.1. In addition, the band-stop frequency can be adjusted in real time to deal with the frequency variation of the grid.

As shown in Fig. 16, a voltage reference vector is limited by a circle rather than the hexagon shown in Fig. 1. This circular limiter can preserve the voltage vector's phase even after its magnitude is limited. The radius of the limiting circle is determined by $\mathrm{MI}_{\max}$, as in

$$|\vec{V}^*|_{\max} = \mathrm{MI}_{\max} \cdot \frac{V_{\mathrm{dc}}}{2} \tag{5}$$

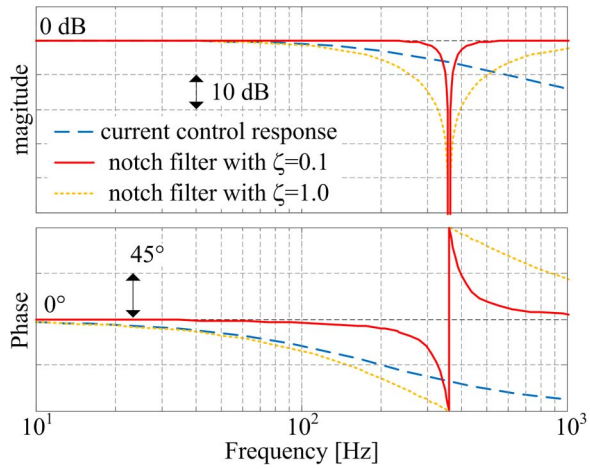

Fig. 18. Bode plots of current control and notch filter.

where $\mathrm{MI}_{\max}$ is the maximum MI allowed to the inverter by considering the harmonic distortions. Up to $\mathrm{MI}_{\max}$, PWM is expected to be linear in terms of the fundamental voltage in the proposed method. Because the harmonic distortion monotonically increases with respect to MI, as shown in Fig. 5, $\mathrm{MI}_{\max}$ can be determined by considering the worst degree of harmonic currents.

In addition to the PI gains of k_p and k_i in (4), the feedback gain denoted by k_r, which is an antiwindup gain, must be specified in Fig. 17. This gain prevents windup of the integrator. From Fig. 17, the following equation can be derived:

$$k_p \cdot i_e + k_i \cdot \frac{\{i_e - k_r(v^* - \bar{v})\}}{s} + \hat{v}_{\mathrm{ff}} = v^* \tag{6}$$

where $\bar{v}$ is the processed output by the circular limiter from voltage reference v^*. $\hat{v}_{\mathrm{ff}}$ indicates feedforwarding voltage.

The controller output v^* can be derived as (7) from (6) as follows:

$$v^* = k_p \cdot i_e + k_i \cdot \frac{(1 - k_r k_p) \cdot i_e + k_r \cdot (\bar{v} - \hat{v}_{\mathrm{ff}})}{s + k_r k_i} + \hat{v}_{\mathrm{ff}}. \tag{7}$$

Because k_r has no meaning if $\bar{v}$ is equal to v^*, (7) holds only when the limiting occurs. Through the midterm in (7), the integrator's response can be explained. If k_r is set to $1/k_p$, distortions caused by i_e can be minimized in the integrator's output. In addition, if the PI gains in (4) are used, (8) can be deduced. Under these settings, the converging response to the limiting value $\bar{v}$ depends only on the system parameter of R/L. That is,

$$v^* = L\omega_{\mathrm{cc}} \cdot i_e + \frac{\frac{R}{L}}{s + R/L} \cdot \bar{v} + \frac{s}{s + R/L} \cdot \hat{v}_{\mathrm{ff}}. \tag{8}$$

When i_e, $\bar{v}$, and $\hat{v}_{\mathrm{ff}}$ are assumed to be step varying, the final value theorem can be applied to (8), to get the steady-state voltage command v^*. In addition, it can be seen that v^* finally converges to $L\omega_{\mathrm{cc}} i_e + \bar{v}$.

This meaning of steady state needs to be extended in the vector space, as shown in Fig. 19. The steady state in the synchronous reference frame means that the previous and present voltage references must be the same. When considering the

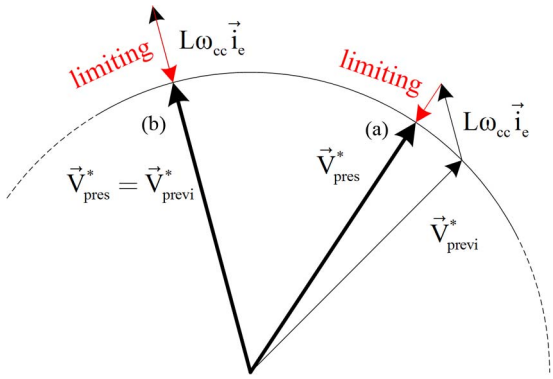

Fig. 19. Voltage reference vector when the limiter works.

cases (a) and (b) in Fig. 19, it can be inferred that those reference vectors are the same only if the direction of current error vector $\vec{i}_e$ is the same with their directions. In other words, the voltage reference vector's direction is driven by the current error vector on the limiting circle to reach the steady state when the limiter works. By the limiting operation, although the magnitude of the current error must not be nullified, the PI controllers for current can still operate to minimize the phase difference between the current vector and its reference. This phase-minimizing operation is effective even under the limiting condition because the circular limiter does not disturb the phase of the voltage reference vector.

IV. Experimental Results

Initially, the proposed method was fundamentally tested with a laboratory-scale prototype inverter. After the current control performance had been confirmed with the prototype, a full-scale inverter was built and tested.

A. Fundamental Operation Under OVM

The small-scale PV inverter was connected to a 110-$V_{\rm rms}$ grid. All the proposed algorithms were implemented in a digital signal processor board based on TMS320F28335. The sampling frequency was 15 kHz, while the switching frequency was 7.5 kHz. The phase-locked loop was based on [19].

To discuss the control dynamics on output currents, the dc-link voltage of the inverter was supplied by a constant voltage source. Initially, when $V_{\rm dc}$ was 179 V, the q-axis current reference was changed in step manner from 5 to 15 A. As presented in Fig. 20, the normal current control response was captured as a reference, while MI was always lower than $1.1547\ (\approx 2/\sqrt{3})$.

For comparison, the same step change with Fig. 20 was tested, when $V_{\rm dc}$ was 159 V. With this dc-link voltage, the inverter operated under OVM after the step change, as shown in Fig. 21. Because harmonic currents increased right after entering into the OVM region, the current control dynamics was not exactly the same with that under the normal modulation. However, in a series of repeated tests, it has been confirmed that the rising time under OVM does not increase when compared to that under the normal modulation.

Although the inverter was under OVM in the test of Fig. 21, the limiter in Fig. 16 set by (5) did not work at all. This means

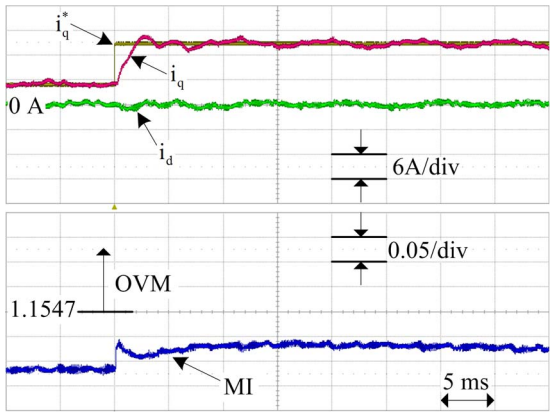

Fig. 20. Current control under normal modulation.

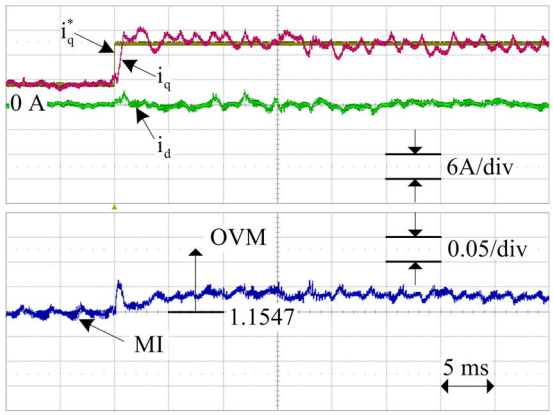

Fig. 21. Current control under OVM.

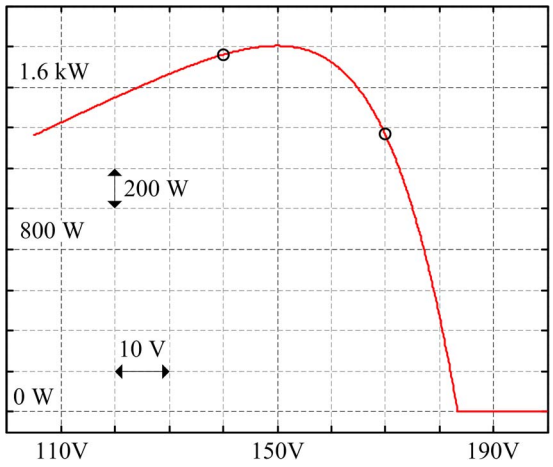

Fig. 22. Power–voltage curve for PV panel emulation.

that the inverter could still synthesize voltage references at the fundamental frequency as intended. It is important to check the proposed method's performance when the voltage output of the inverter is saturated.

In order to consider the circular limiter's transient operation, the dc link of the inverter was connected to a PV simulator that emulated the power–voltage curve of a solar panel shown in Fig. 22. At the beginning, the inverter regulated its dc-link

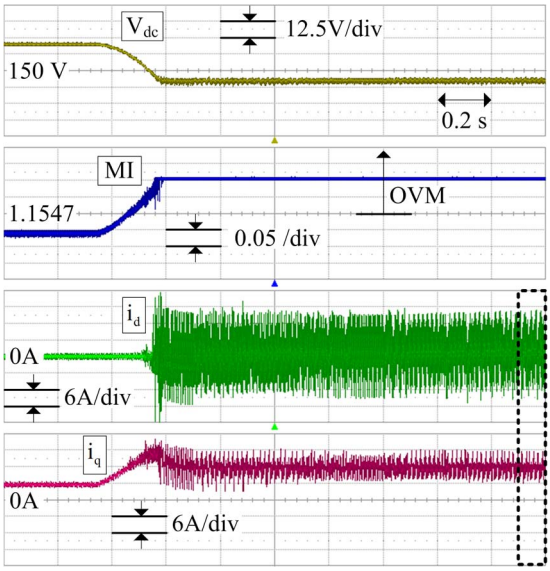

Fig. 23. Circular limiter test.

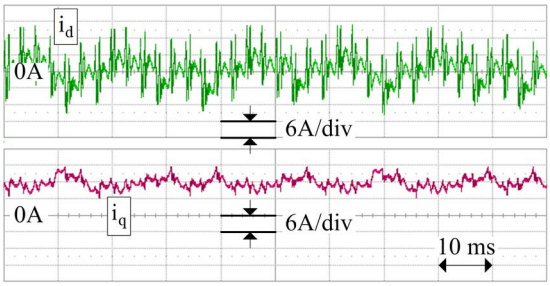

Fig. 24. Magnified current waveforms of Fig. 23.

voltage as 170 V. When MI_{max} was set to 1.26 in (5), the dc-link voltage was decreased toward 140 V, with the rate of 150 V/s, as shown in Fig. 23.

The dc-link voltage was settled down to 143 V, whereas its reference was 140 V. In result, the MI was reached to its preset maximum value of 1.26 in steady state, as shown in Fig. 23. This fact indicates that the magnitude of voltage output was limited by the proposed limiting method. The dashed box in Fig. 23 has been magnified in Fig. 24 to carefully investigate the output currents. Although lots of harmonics were included, the average of d-axis current was still regulated as 0.64 A, which almost coincided with its reference to keep unity power factor. This means that the proposed method is able to maintain the power factor of fundamental currents, as expected, even if the limiter operates.

B. Discussion on Data From Gochang Proving Ground

The proposed method under OVM has been tested in a 250-kW PV inverter connected to PV panels in the Gochang PV generation proving ground, South Korea. The inverter and PV panels are shown in Fig. 25. In fact, for higher efficiency, the PV inverter is based on T-type three-level topology shown in Fig. 26. However, if the three-level inverter is under OVM, it is hard to use the small vectors [20]. This can cause instability

Fig. 25. 250-kW PV inverter and Gochang proving ground.

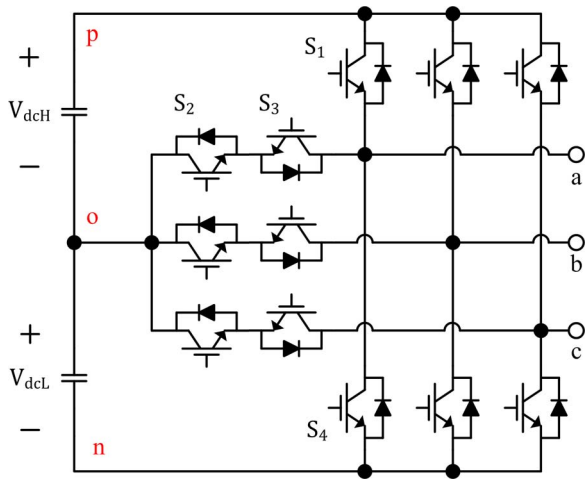

Fig. 26. T-type three-level inverter.

in the neutral potential control. Because the T-type inverter is a type of hybrid topology, it can be also operated as the two-level inverter by opening the switches connecting the neutral points. Through this two-level operation, the PV inverter under test can operate under OVM.

The test data have been obtained on February 28, 2014, and the weather was cloudy. Because the temperature around sunset was about 6 °C, the open circuit voltage of PV panels was relatively high when compared to a 280-V_{rms} grid where the inverter was connected. The OVM by the proposed method has been briefly observed on that day. Test data have been logged by analyzing instruments.

As shown in Fig. 27, the inverter continued to transfer power from PV panels to the grid, even if the dc-link voltage was decreased due to sunset. Because 450 V was officially the lower limit for MPPT in the inverter's catalogue, the electrical energy from the PV generation after 17:50, i.e., about 234 Wh, comes from the proposed system operation. The variation of MI up to the preset MI_{max} of 1.223 can be sequentially confirmed in Fig. 28. When considering Figs. 27 and 28, it can be inferred that the inverter entered into the OVM region near 420 V (around 17:55).

It is important to check the harmonic distortions of output currents, as shown in Fig. 29. Although data associated with harmonic distortions in the figure were not smoothly obtained due to some measuring errors, the distortion trend could be roughly identified. Then, the inverter would have complied with

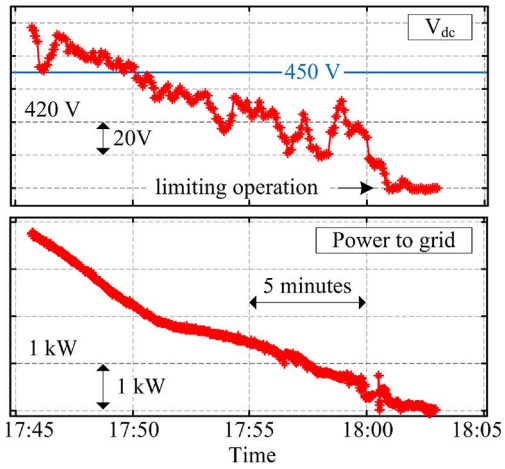

Fig. 27. DC-link voltage and generated power around sunset.

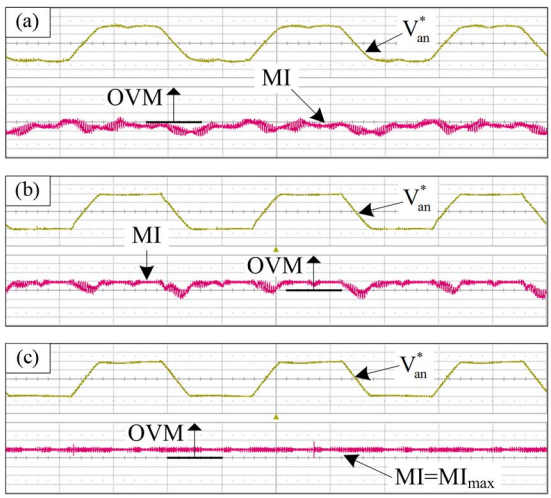

Fig. 28. Pole voltage reference and MI at (a) 17:55, (b) 18:00, and (c) 18:02 (V^*_{an}: 100 V/div with center at 0 V; MI: 0.075/div with center at 1.1547; time: 5 ms/div).

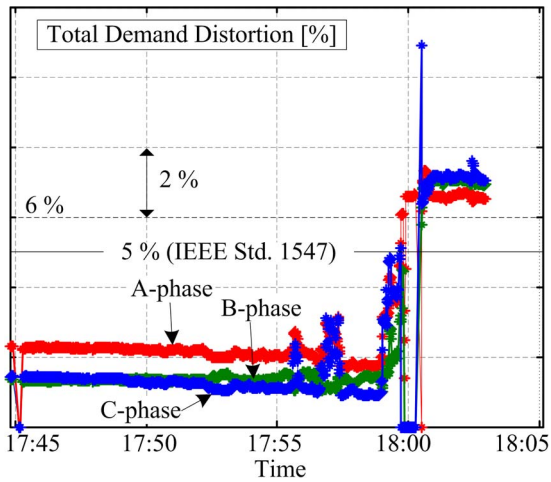

Fig. 29. Total demand distortion for each phase current around sunset.

IEEE std. 1547 at the total demand distortion if MI_{max}, which determines the radius of the limiting circle in Fig. 16, had been modified aptly smaller than 1.223. This is because the harmonic distortion increases as MI increase under OVM, as shown in Fig. 5. On the basis of Figs. 27 and 29, 400 V is deemed a minimum voltage for the inverter's dc link at the proving ground with the proposed OVM. That is, the proposed method could expand the MPPT range by decreasing the minimum voltage by 11.1%, from 450 to 400 V. However, a trial-and-error approach could be necessary to set MI_{max} for the application of the proposed method because harmonic distortions also depend on the circumstance where a PV inverter is installed.

V. Conclusion

In this paper, an OVM strategy has been proposed for the grid-connected PV inverter. Initially, OVM methods have been designed to linearly modulate the fundamental voltage according to its reference. In conjunction with this linear OVM, the circular limiter has been utilized instead of a voltage hexagon. The settings for current control have been carefully detailed, so that the current control property is kept even under OVM. After the proposed method's fundamental operations were tested in a small-scale inverter, its feasibility was examined with a 250-kW PV generation system in a proving ground. Although the weather condition was not optimal to extensively test the proposed method, it has been confirmed that the PV inverter can execute MPPT at very low dc-link voltages through the proposed method, without unnecessary stall. Due to the proposed control method, the operation time of the PV inverter has been extended by 12 min, and the generated energy has been increased by 234 Wh around sunset on the day of concern.

References

[1] J. Holtz, W. Lotzkat, and A. M. Khambadkone, "On continuous control of PWM inverters in the overmodulation range including the six-step mode," *IEEE Trans. Power Electron.*, vol. 8, no. 4, pp. 546–553, Oct. 1993.

[2] A. M. Khambadkone and J. Holtz, "Compensated synchronous PI current controller in overmodulation range and six-step operation of space-vector-modulation-based vector-controlled drives," *IEEE Trans. Ind. Electron.*, vol. 49, no. 3, pp. 574–580, Jun. 2002.

[3] D. R. Seidl, D. A. Kaiser, and R. D. Lorenz, "One-step optimal space vector PWM current regulation using a neural network," in *Conf. Rec. IEEE IAS Annu. Meeting*, Oct. 2–6, 1994, pp. 867–874.

[4] L. Rossetto, P. Tenti, and A. Zuccato, "Integrated optimum control of quasi-direct converters," *IEEE Trans. Power Electron.*, vol. 12, no. 6, pp. 993–999, Nov. 1997.

[5] J.-K. Seok, J.-S. Kim, and S.-K. Sul, "Overmodulation strategy for high-performance torque control," *IEEE Trans. Power Electron.*, vol. 13, no. 4, pp. 786–792, Jul. 1998.

[6] B.-H. Bae and S.-K. Sul, "A novel dynamic overmodulation strategy for fast torque control of high-saliency-ratio AC motor," *IEEE Trans. Ind. Appl.*, vol. 41, no. 4, pp. 1013–1019, Jul./Aug. 2005.

[7] A. M. Hava, R. J. Kerkman, and T. A. Lipo, "Carrier-based PWM-VSI overmodulation strategies: Analysis, comparison, and design," *IEEE Trans. Power Electron.*, vol. 13, no. 4, pp. 674–689, Jul. 1998.

[8] A. M. Hava, S.-K. Sul, R. J. Kerkman, and T. A. Lipo, "Dynamic overmodulation characteristics of triangle intersection PWM methods," *IEEE Trans. Ind. Appl.*, vol. 35, no. 4, pp. 896–907, Jul./Aug. 1999.

[9] K. Zhou and D. Wang, "Relationship between space-vector modulation and three-phase carrier-based PWM: A comprehensive analysis," *IEEE Trans. Ind. Electron.*, vol. 49, no. 1, pp. 186–196, Feb. 2002.

[10] *IEEE Standard for Interconnecting Distributed Resources With Electric Power Systems*, IEEE Std. 1547, 2003.

[11] Y. Peng, D. Vrancic, and R. Hanus, "Anti-windup, bumpless, and conditioned transfer techniques for PID controllers," *IEEE Control Syst. Mag.*, vol. 16, no. 4, pp. 48–57, Aug. 1996.

[12] H. W. V. D. Broeck, H.-C. Skudelny, and G. V. Stanke, "Analysis and realization of a pulsewidth modulator based on voltage space vectors," *IEEE Trans. Ind. Appl.*, vol. 24, no. 1, pp. 142–150, Jan./Feb. 1988.
[13] D. G. Holmes and T. A. Lipo, "Choice of performance indicator," in *Pulse Width Modulation for Power Converters*. Hoboken, NJ, USA: Wiley, 2003, ch. 2.4, pp. 67–70.
[14] D.-W. Chung, "Unified analysis of PWM method for three phase voltage source inverter using offset voltage," Ph.D. dissertation, Seoul Nat. Univ., Seoul, Korea, 2000.
[15] F. Briz, A. Diez, M. W. Degner, and R. D. Lorenz, "Current and flux regulation in field-weakening operation," *IEEE Trans. Ind. Appl.*, vol. 37, no. 1, pp. 42–50, Jan./Feb. 2001.
[16] Generating plants connected to the medium-voltage network, Bundesverband der Energie-und Wasserwirtschaft (BDEW), Berlin, Germany, BDEW tech. guid., Jun. 2008.
[17] S.-K. Sul, "Design of regulators for electric machines and power converters," in *Control Electric Machine Drive Systems*. Hoboken, NJ, USA: Wiley, 2011, ch. 4, pp. 154–229.
[18] R. Teodorescu, F. Blaabjerg, M. Liserre, and P. C. Loh, "Proportional-resonant controllers and filters for grid-connected voltage-source converters," *Proc. Inst. Elect. Eng.—Elect. Power Appl.*, vol. 153, no. 5, pp. 750–762, Sep. 2006.
[19] Y. Park, S.-K. Sul, W.-C. Kim, and H.-Y. Lee, "Phase locked loop based on an observer for grid synchronization," *IEEE Trans. Ind. Appl.*, vol. 50, no. 2, pp. 1256–1265, Mar./Apr. 2014.
[20] Y. Park, S.-K. Sul, C.-H. Lim, W.-C. Kim, and S.-H. Lee, "Asymmetric control of DC-link voltages for separate MPPTs in three-level inverters," *IEEE Trans. Power Electron.*, vol. 28, no. 6, pp. 2760–2769, Jun. 2013.

Yongsoon Park (S'12–M'15) received the B.S., M.S., and Ph.D. degrees from Seoul National University, Seoul, Korea, in 2008, 2010, and 2015, respectively, all in electrical engineering.

He is currently a Senior Engineer with Samsung Electronics Company, Ltd., Suwon, Korea. His current research interests include sensorless drives of electrical machines and power conversion circuits.

Seung-Ki Sul (S'78–M'87–SM'98–F'00) was born in Korea in 1958. He received the B.S., M.S., and Ph.D. degrees from Seoul National University, Seoul, Korea, in 1980, 1983, and 1986, respectively, all in electrical engineering.

From 1986 to 1988, he was an Associate Researcher with the Department of Electrical and Computer Engineering, University of Wisconsin, Madison, WI, USA. From 1988 to 1990, he was a Principal Research Engineer with LG Industrial Systems Company, Korea. Since 1991, he has been a member of the faculty in the School of the Electrical and Computer Engineering, Seoul National University, where he is currently a Professor. He has been actively involved in various industry projects sponsored by many Korean, Japanese, and American companies. He has over 130 IEEE journal papers and a total of more than 300 international conference papers in the area of power electronics. He holds 14 U.S. patents, seven Japanese patents, and 11 Korean patents, and he has granted 41 Ph.D. students under his supervision. His current research interests include power electronic control of electrical machines, electric/hybrid vehicles and ship drives, high-voltage dc transmission based on modular multilevel converters, and power-converter circuits for renewable energy sources. He is one of the pioneers in the area of carrier-based pulsewidth modulation (PWM) technology applied to the control of the power converters. From 2005 to 2007, he was the Vice Dean of the Engineering College of Seoul National University. In addition, from 2008 to 2011, he was the President of the Electrical Engineering Science Research Institute funded by the Korean Government. For his sabbatical year from 2003 to 2004, he served as an acting Director of the research center of Yaskawa Electric Company, Japan. From 1998 to 2003, he was a Board Member of Hyundai Elevator Company, which is the largest elevator maker in Korea. From 2011 to 2014, he was a Board Member of LS Industrial System Co., which is the largest power-electronics-related product maker in Korea.

Prof. Sul was the Program Chair of the 2006 IEEE Power Electronics Specialists Conference (PESC'06) and the General Chair of the IEEE Energy Conversion Congress and Exposition Asia and International Conference on Power Electronics, in 2011. For the last three years, he has served as the Editor-in-Chief of the *Journal of Power Electronics*, which is registered in Science Citation Index Expanded, published by the Korean Institute of Power Electronics (KIPE), Seoul, Korea. Since 2015, he has been the President of KIPE.

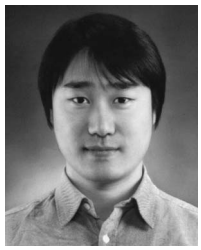

Ki-Nam Hong was born in Korea in 1979. He received the B.S. and M.S. degrees in embedded software engineering from Kwangwoon University, Seoul, Korea, in 2007 and 2012, respectively.

From 2008 to 2009, he was an Engineer with TmaxSoft, Inc., Gyeonggi, Korea. From 2012 to 2015, he was an Associate Research Engineer with LG Uplus, Inc., Seoul, Korea. Since 2015, he has been with LG Electronics, Inc., Incheon, where he is currently an Associate Research Engineer with the Incheon R&D Center. His main research interests include power electronic control of renewable energy.